

See discussions, stats, and author profiles for this publication at: <https://www.researchgate.net/publication/311567548>

Oxygen transportation, electrical conductivity and electrochemical properties of layered perovskite $\text{SmBa}_{0.5}\text{Sr}_{0.5}\text{Co}_2\text{O}_{5+\delta}$

Article in International Journal of Hydrogen Energy · December 2016

DOI: 10.1016/j.ijhydene.2016.11.123

CITATIONS

0

READS

20

3 authors, including:



Adi Subardi

National Dong Hwa University

8 PUBLICATIONS 19 CITATIONS

[SEE PROFILE](#)



Yen-Pei Fu

National Dong Hwa University

139 PUBLICATIONS 1,673 CITATIONS

[SEE PROFILE](#)



ELSEVIER

Available online at www.sciencedirect.com**ScienceDirect**journal homepage: www.elsevier.com/locate/he

CrossMark

Oxygen transportation, electrical conductivity and electrochemical properties of layered perovskite $\text{SmBa}_{0.5}\text{Sr}_{0.5}\text{Co}_2\text{O}_{5+\delta}$

Adi Subardi ^{a,b}, Ching-Cheng Chen ^a, Yen-Pei Fu ^{a,c,*}^a Department of Materials Science & Engineering, National Dong Hwa University, Shou-Feng, Hualien 97401, Taiwan^b Department of Mechanical Engineering, STTNAS, Yogyakarta 55281, Indonesia^c Nanotechnology Research Center, National Dong Hwa University, Shou-Feng, Hualien 97401, Taiwan**ARTICLE INFO****Article history:**

Received 4 September 2016

Received in revised form

2 November 2016

Accepted 17 November 2016

Available online 10 December 2016

Keywords:

Solid oxide fuel cells

Layered perovskite

Oxygen permeation

Exchange current density

Long-term testing

ABSTRACT

Oxygen transportation properties of $\text{SmBa}_{0.5}\text{Sr}_{0.5}\text{Co}_2\text{O}_{5+\delta}$ (SBSC55) layered perovskite has been investigated as a potential cathode for intermediate-temperature solid oxide fuel cells (IT-SOFCs). This research includes the following items: (1) structural characteristics, thermogravimetric behavior, oxygen permeation, chemical bulk diffusion coefficient (D_{chem}), and (2) the electrochemical performance of long-term testing carried out to evaluate its electrochemical stability. The D_{chem} values for SBSC55 cathode are 2.6×10^{-6} , 9.1×10^{-6} and $1.8 \times 10^{-5} \text{ cm}^2 \text{ s}^{-1}$ at 500 °C, 600 °C, and 700 °C, respectively. The oxygen permeation flux for SBSC55 membrane with 1.0 mm thickness increased from $0.143 \text{ mL min}^{-1} \text{ cm}^{-2}$ at 500 °C to $0.406 \text{ mL min}^{-1} \text{ cm}^{-2}$ at 800 °C under synthetic air at a flow rate of 50 mL min^{-1} , helium at a rate of 25 mL min^{-1} . The activation energies of oxygen permeation for the high temperature region (700–800 °C) and low temperature region (500–650 °C) are 23.67 and 6.96 kJ mol⁻¹, respectively. It suggested that oxygen diffusion for high temperature range is surface exchange process, low temperature range is bulk diffusion process. The long-term test of cathodic polarization resistance for SBSC55|SDC|SSBSC55 half-cell at 600 °C during 96 h has been carried out with an increase rate of 0.30% h⁻¹. Based on the impedance spectra with various oxygen partial pressure results, the rate-limiting process of ORR is determined that the oxygen ion transfer from triple-phase boundary (TPB) and/or two-phase boundary (2PB) sites of cathode is major with the minority of charger transfer reaction.

© 2016 Hydrogen Energy Publications LLC. Published by Elsevier Ltd. All rights reserved.

Introduction

Solid-oxide fuel cells (SOFCs) have the prospective for being one of the cleanest and quite a few effective energy for direct transformation of chemical fuels to electricity [1]. The high

operating temperature limit the application of SOFCs such as using expensive materials to endure high temperature, while lower operating temperature leads to sluggish oxygen reduction kinetics and high over-potential at the cathode [2,3]. A lower operating temperature can reduce problems with sealing and thermal degradation, and allow the use of low-cost metal

* Corresponding author. Department of Materials Science & Engineering, National Dong Hwa University, Shou-Feng, Hualien 97401, Taiwan. Fax: +886 3 863 4200.

E-mail address: ypfu@mail.ndhu.edu.tw (Y.-P. Fu).

<http://dx.doi.org/10.1016/j.ijhydene.2016.11.123>

0360-3199/© 2016 Hydrogen Energy Publications LLC. Published by Elsevier Ltd. All rights reserved.

interconnection materials, and suppress reactions between the cell components, thus lowering the cost of SOFCs. However, the electrochemical activity of the cathode dramatically decreases with decreasing temperature. Generally, the cathode becomes the confining factor in identifying the overall cell performance. Therefore, the exploitation of new electrodes with higher electrocatalytic activities is critical for IT-SOFCs [4,5]. The high performance cathodes with regard to IT-SOFCs mainly based on perovskite structure and its derivative structures. The cobaltites with prominent electrochemical properties have been investigated for IT-SOFC cathode applications [6–8]. They are notable for their superb mixed-ionic-and-electronic conductor (MIEC) performance in the intermediate temperature range. Recently, there have been some reports concerning the impressive oxygen reduction reaction (ORR) for oxygen-deficient layered perovskites. They are suitable for application as cathodes in IT-SOFCs, which require faster oxygen diffusion rates as well as higher surface exchange kinetics at intermediate temperatures range [9–11].

A-site ordered perovskites, $\text{LnBaCo}_2\text{O}_{5+\delta}$, oxygen can easily migrate through the LnO plane, which was observed via neutron diffraction technique and molecular dynamics simulations [12–14]. In order to improve the oxygen mobility in the LnO plane, many researchers tried to dope different lanthanides and alkali-earth metals into the A-site of oxygen-deficient layered perovskites such as $\text{NdBa}_{1-x}\text{Sr}_x\text{Co}_2\text{O}_{5+\delta}$ [15], $\text{GdBa}_{0.5}\text{Sr}_{0.5}\text{Co}_{2-x}\text{Fe}_x\text{O}_{5+\delta}$ [16,17], $\text{PrBa}_{0.5}\text{Sr}_{0.5}\text{Co}_{2-x}\text{Fe}_x\text{O}_{5+\delta}$ [18], $\text{YBa}_{0.6}\text{Sr}_{0.4}\text{Co}_2\text{O}_{5+\delta}$ [19], $\text{SmBa}_{0.5}\text{Sr}_{0.5}\text{Co}_2\text{O}_{5+\delta}$ [20–23]. Mckinlay et al. reported that the substitution of Sr for Ba resulted in a significant increase of conductivity in $\text{YBaCo}_2\text{O}_{5+\delta}$. The conductivity value of $\text{YBa}_{0.5}\text{Sr}_{0.5}\text{Co}_2\text{O}_{5+\delta}$ is much higher than $\text{YBaCo}_2\text{O}_{5+\delta}$, presumably due to the smaller lattice volume for Sr-substituted specimen [24]. Kim et al. proposed that substitution of Sr for Ba in $\text{GdBaCo}_2\text{O}_{5+\delta}$ improved chemical stability between the cathode and electrolyte, and expedited oxygen transport [25]. Meng et al. reported that Sr doping in $\text{YBaCo}_2\text{O}_{5+\delta}$ enhance the electrical conductivity possibly due to the greater amount of electronic holes and mobile interstitial oxygen [26]. Based on the above-mentioned reports, it concludes that the substitution of Sr^{2+} for Ba^{2+} site results in higher electrical conductivity as well as better electrochemical performance of layered perovskites.

In this study, the layered perovskite, $\text{SmBa}_{0.5}\text{Sr}_{0.5}\text{Co}_2\text{O}_{5+\delta}$ (SBSC55), is chosen as a cathode material. The crystal structure, thermogravimetric property, oxygen non-stoichiometry, oxygen permeation, electrical properties, and electrochemical properties with long-term testing have been investigated. Moreover, to evaluate the oxygen-transportation property, the oxygen permeation measurement was carry out. Base on the test, it is easy for us to look into the cathode if it is suitable as a cathode for SOFC.

Experimental

Cathode and electrolyte materials preparation

Stoichiometric amounts of Sm_2O_3 , SrCO_3 , BaCO_3 and CoO (powders were used as starting materials). The $\text{SmBa}_{0.5}\text{Sr}_{0.5}\text{Co}_2\text{O}_{5+\delta}$ (SBSC55) cathode powders were prepared

via the solid-state reaction. The ball-milled mixture was dried and ground into a powder with mortar and pestle, and then calcined in air at 1100 °C for 4 h [27]. The $\text{Ce}_{0.8}\text{Sm}_{0.2}\text{O}_{1.9}$ (SDC) powder was synthesized by co-precipitation using $\text{Ce}(\text{N-O}_3)_3 \cdot 6\text{H}_2\text{O}$ and $\text{Sm}(\text{NO}_3)_3 \cdot 6\text{H}_2\text{O}$ as the starting materials. These starting materials with stoichiometric ratio were dissolved in distilled water and then added to a solution of ammonia. The pH value of the solution was adjusted to 9.5–10. Then, the coprecipitation powder was calcined in air to 600 °C for 2 h. The detailed procedure regarding the preparation of SDC can refer to Ref. [28].

Material characterization

The structure the sintered SBSC55 cathode was characterized by X-ray powder diffractometer (XRD; Rigaku D/MAX-2500V), with a scanning rate of 4°/min and scanning range of 20–80°, using a Cu K_α (1.5418 Å) radiation source. The powder pattern and lattice parameter were analyzed by Rietveld refinement. The microstructures of the SBSC55 cathode were observed by scanning electron microscope (SEM; Hitachi 3500H). Thermogravimetric properties of SBSC55 cathode powder was performed by a thermogravimetric analyzer (TGA, SII TG/DTA 6300) at various oxygen partial pressure, $p(\text{O}_2) = 0.20, 0.10, 0.03, 0.01$ and 3.20×10^{-3} atm. Controlled $p(\text{O}_2)$ values were generated by use of O_2-N_2 gas mixture using a total flow rate of 100 mL min⁻¹, and $p(\text{O}_2)$ monitored with a zirconia-based oxygen sensor. The weight loss of SBSC55 measured at $p(\text{O}_2) = 0.2$ atm is used to evaluate amount of desorption oxygen. The oxygen non-stoichiometry (δ) with varying $p(\text{O}_2)$ and temperature was calculated from the following equation [29].

$$\Delta\delta = \frac{M_s \Delta m}{M_o m} \quad (1)$$

where $\Delta\delta$ is the change in oxygen content, M_s is the molar mass of the sample, M_o is the molar mass of oxygen, Δm is the sample mass change after being heated, m is the sample mass at room temperature, m is the sample mass at room temperature, and the room temperature oxygen non-stoichiometry was determined by iodometric titration [30].

Electrical conductivity relaxation technique

The electrical conductivity relaxation was measured by the four-probe DC method, where two silver wires acting as current leads and two other silver wires acting as voltage probes were attached to the electrodes. A constant current was delivered to the two current wires, and the voltage response was recorded by a digital source meter (Keithley 2420). Measurement was performed on a specimen with a rectangular geometry, having typical size of $5 \times 5 \times 10$ mm³ and above 95% of the theoretical density over the temperature range of 500–700 °C at an interval of 50 °C. After each temperature change, the bar was stabilized for at least 30 min. A sudden change at $p(\text{O}_2)$, from 0.05 to 0.21 atm was caused by introducing standard gas mixtures of Ar and O₂. Small oxidation and reduction steps were alternatively applied to study the D_{chem} . Typically, a sequence of several reduction/oxidation cycles was performed at each temperature. The electrical

conductivity relaxation curve was plotted as $\frac{\sigma(t)-\sigma(0)}{\sigma(\infty)-\sigma(0)}$ versus t. The values for D_{chem} could be determined by fitting the ECR curves. The experimental details have been reported in an earlier publication [31].

Oxygen permeation measurement

Oxygen permeation properties of SBSC55 membrane was measured using an in-house oxygen permeation set-up as shown in Fig. 1. As for the membrane preparation is described as follows. The ball-milled calcined SBSC55 powder was press-formed into a disk diameter 13 mm and sintered at 1000 for 4 h in air. The SBSC55 membrane for oxygen permeation test was polished to thickness of 1.0 mm and sealed with gold ring between two quartz rods. The feed side fed with synthetic air ($21 \text{ vol\% O}_2 + 79 \text{ vol\% N}_2$) at a flow rate of 50 mL min^{-1} , while high pure helium was applied to sweep side at a flow rate of 25 mL min^{-1} . An online-coupled Agilent 7890 gas chromatograph with a RT-Msieve 5A column was used to analyze the concentration of nitrogen and oxygen. The oxygen permeation flux was determined by the following equation [32].

$$J(O_2) = \left(C_{O_2} - \frac{0.21}{0.79} \sqrt{\frac{28}{32}} C_{N_2} \right) \frac{F}{S} \quad (2)$$

where $J(O_2)$ is the oxygen permeation flux ($\text{mL min}^{-1} \text{cm}^{-2}$), where C_{O_2} and C_{N_2} are the measured gas-phase concentrations in percentage of oxygen and nitrogen in the penetrative stream, respectively, F is the flow rate (mL min^{-1}) of the sweeping gas, and S is the effective surface area (cm^2) of the disk exposed to the sweeping gas. The measurement was conducted over a temperature range of $500\text{--}800^\circ\text{C}$.

Symmetrical cell fabrication and measurement

A symmetrical cell of SBSC55|SDC|SBSC55 configuration was fabricated by screen-printing technique. The SBSC55 cathode was pasted on both sides of SDC electrolyte discs in circles of 13 mm diameter and 1 mm thick. After the SBSC55 cathode was painted on the SDC electrolyte, it was sintered at 1000°C

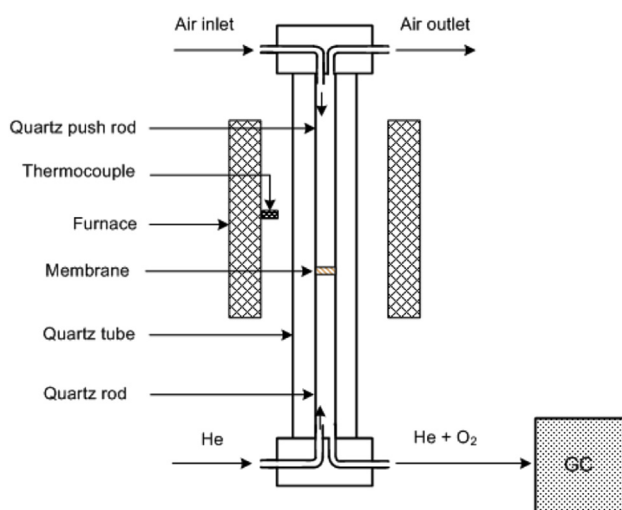


Fig. 1 – Schematic of oxygen permeation set-up.

for 4 h in air. The SBSC55 cathode was used as the working electrode (WE) with surface area of 0.385 cm^2 . The Ag reference electrode (RE) was placed away from the WE by about $0.3\text{--}0.4 \text{ cm}$. The SBSC55 cathode counter electrode (CE) was placed on the other side of the SDC disk.

The symmetrical testing cell experiments were carried out under various oxygen partial pressures in temperatures ranging from 600 to 800°C at intervals of 50°C in a tube-furnace. The AC impedance measurement was performed using the VoltaLab PGZ301 potentiostat with frequency applied range from 100 kHz to 0.1 Hz with 10 mV AC signal amplitude. Under the cathodic polarized condition, the electrochemical impedance spectrometry (EIS) was conducted as a function of the applied cathodic voltage. For long-term testing, EIS was measured at 600°C during 96 h in air. The EIS fitting analysis was performed with the Z-view software. The Linear sweep voltammetry was measured between -0.4 and 0.1 V with sweep rate 0.5 mV s^{-1} versus the RE.

Result and discussion

Crystal structure

The XRD pattern of SBSC55 calcined at 1100°C for 4 h showed in Fig. 2(a). Obviously, the SBSC55 revealed the double-perovskite structure without any peaks attributable to impurities. The Rietveld refinement of SBSC55 including the measured, the calculated profile, and the difference between them depicted in Fig. 2(b). The experimental data and the calculated profiles are wonderful agreement, and it revealed that the cations are well ordered between Sm^{3+} and $\text{Ba}^{2+}/\text{Sr}^{2+}$ ions in the ordered perovskite lattice [33]. The Rietveld refinement data reveal that the diffraction pattern of SBSC55 could be indexed to a tetragonal structure as listed in Table 1 with space group: $P4/mmm$, lattice parameter: $a = 3.88 \text{ \AA}$, $b = 3.88 \text{ \AA}$, $c = 7.58 \text{ \AA}$, and $v = 114.30 \text{ \AA}^3$. In SBSC55 structure, Sm atoms are located at $1a$ (0, 0, 0) sites, Ba and Sr are distributed at random over the $1b$ (0, 0, 0.5) sites. While Co atoms are placed at $2h$ (0.5, 0.5, 0.25) sites and O atoms are randomly located at $4i$ (0, 0.5, 0.27), $1c$ (0.5, 0.5, 0), and $2h$ (0.5, 0.5, 0.44) sites.

Chemical bulk diffusion coefficient (D_{chem})

The electrode performance is highly related to the intrinsic properties of the electrode material such as bulk diffusion and surface exchange kinetics properties. In present research, D_{chem} was measured by an ECR technique based on the principle that a variation in the ambient atmosphere leads to a change in the oxygen vacancy concentration of the MIEC. Due to the local electroneutrality requirement, the abrupt change in the $p(O_2)$ of the surrounding atmosphere induces a corresponding change of the charge carrier concentration (oxygen vacancy), which is reflected as a relaxation of the apparent macroscopic electrical conductivity. Conductivity relaxation models usually assume small departures from thermal equilibrium and a simple linear model for the surface exchange kinetics [34]. Fig. 3(a) shows the electrical conductivity relaxation curves of SBSC55 at various temperatures by a sudden

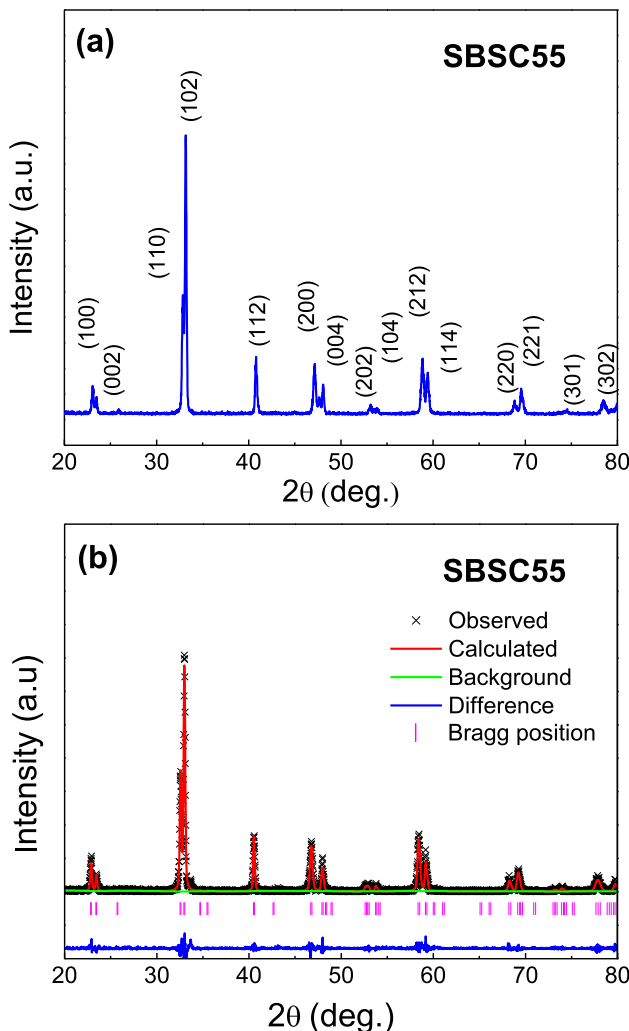


Fig. 2 – (a) X-ray powder diffraction pattern and **(b)** Rietveld refinement of SBSC55 calcined at 1100 °C for 4 h. Observed (cross symbols), calculated (solid line) XRD profiles and the difference (bottom line) between them.

change at $p(O_2)$ from 0.21 to 0.05 atm. The elemental steps for the oxygen exchange could be considered as (i) surface reaction that involves ionization of oxygen or deionization of oxide ions at the gas/solid interface and (ii) diffusion in solid specimen. In a solid, movement of oxide ions is counterbalanced by a simultaneous motion of electron holes, which is characterized as a chemical diffusion process.

Table 1 – Crystallographic data of SBSC55 from the Rietveld refinement.^a

Atom	Wyckoff position	x	y	z	Uiso
Sm1	1a (0 0 0)	0	0	0	0.0146
Co2	2h ($\frac{1}{2}$ $\frac{1}{2}$ z)	0.5	0.5	0.2534	0.0007
Ba3/Sr3	1b (0 0 $\frac{1}{2}$)	0	0	0.5	0.0062
O4	4i (0 $\frac{1}{2}$ z)	0	0.5	0.2678	0.0177
O5	1c ($\frac{1}{2}$ $\frac{1}{2}$ 0)	0.5	0.5	0	0.0098
O6	2h ($\frac{1}{2}$ $\frac{1}{2}$ z)	0.5	0.5	0.4411	0.0304

^a Space group: P4/mmm, tetragonal structure, $a = 3.88 \text{ \AA}$, $b = 3.88 \text{ \AA}$, $c = 7.58 \text{ \AA}$, $v = 114.30 \text{ \AA}^3$, $R_p = 1.81$, $R_{wp} = 2.80\%$, $R_{exp} = 2.72\%$.

The conductivity reached its steady state value and faster for high temperatures than low temperatures, leading to the fact that D_{chem} at high temperatures was larger than one at low temperature. D_{chem} values of SBSC55 measured via ECR technique are 2.6×10^{-6} , 9.1×10^{-6} , and $1.8 \times 10^{-5} \text{ cm}^2 \text{ s}^{-1}$ at 500 °C, 600 °C, and 700 °C, respectively. There are some previous studies regarding D_{chem} values determined by ECR methods [35–38]. For single perovskites, the D_{chem} values of $\text{Ba}_{0.6}\text{Sr}_{0.4}\text{Co}_{0.9}\text{Nb}_{0.1}\text{O}_{3-\delta}$ ranged from $1.2 \times 10^{-5} \text{ cm}^2 \text{ s}^{-1}$ at 450 °C to $1.3 \times 10^{-6} \text{ cm}^2 \text{ s}^{-1}$ at 600 °C [35]. Chen et al. [36] reported that D_{chem} values of $\text{Ba}_{0.5}\text{Sr}_{0.5}\text{Co}_{0.8}\text{Fe}_{0.2}\text{O}_{3-\delta}$ are between 2.5×10^{-5} and $3.9 \times 10^{-4} \text{ cm}^2 \text{ s}^{-1}$ for temperatures between 600 and 800 °C; similarly, the D_{chem} values of the of $\text{La}_{0.1}\text{Sr}_{0.9}\text{Co}_{0.8}\text{Fe}_{0.2}\text{O}_{3-\delta}$ is $1.85 \times 10^{-5} \text{ cm}^2 \text{ s}^{-1}$ at 650 °C [37]. For double perovskite, Kim et al. presented that D_{chem} values of $\text{PrBaCo}_2\text{O}_{5+\delta}$ are between 3×10^{-6} and $5 \times 10^{-5} \text{ cm}^2 \text{ s}^{-1}$ for temperatures between 300 and 500 °C [38]. The variance between the previous paper and this work is attributed to the different procedures applied during the ECR measurement or the variation between sample compositions especially crystallinity and stoichiometry.

The activation energy of D_{chem} for SBSC55 is $57.96 \text{ kJ mol}^{-1}$ calculated by the Arrhenius plot of D_{chem} vs. $1000/T$ as shown in Fig. 3(b). The equation of D_{chem} as a function of reciprocal

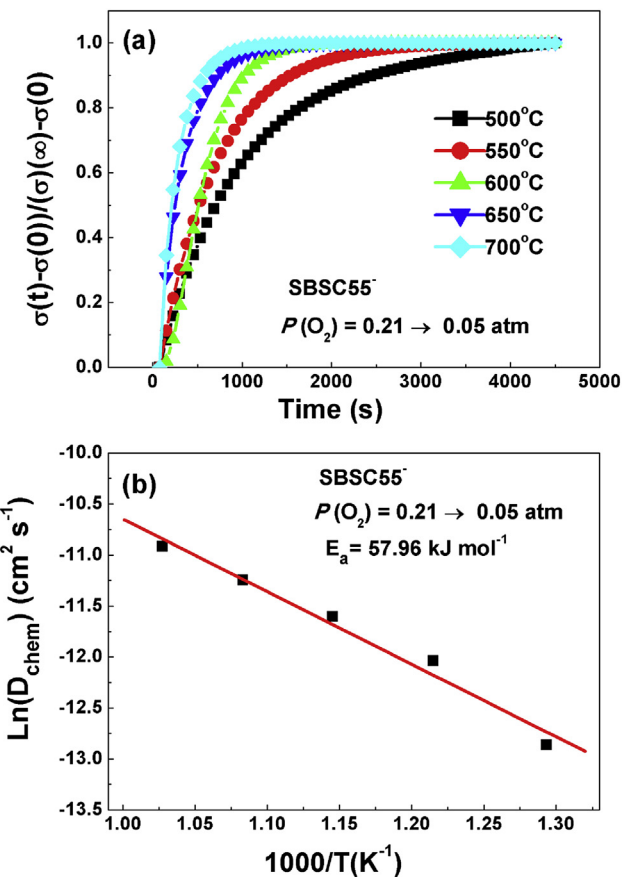


Fig. 3 – (a) Normalized conductivity relation plots for SBSC55 for reduction step change in oxygen pressure with a final oxygen pressure of 0.05 atm; **(b)** Arrhenius plot of D_{chem} vs. $1000/T$ for SBSC55 cathode ranged from 500 to 700 °C.

temperature calculated from the in the temperature range of 500–700 °C exhibits as follow:

$$D_{\text{chem}} = 1.92 \times 10^{-5} \exp\left(-\frac{57.96 (\text{kJ mol}^{-1})}{RT}\right) (\text{m}^2 \text{s}^{-1}) \quad (3)$$

The activation energy obtained from the Arrhenius plot of D_{chem} vs. $1000/T$ may be considered in terms of the enthalpy of mobility of the defects involved in the gas/solid equilibration for the $\text{O}_2/\text{SBSC55}$ system. This behavior is considered to result from the effect of $p(\text{O}_2)$ is significantly related to the concentration of defects and the extent of interactions between the defects and their mobility [36].

Oxygen permeation

The temperature dependence of the oxygen permeation flux (J_{O_2}) for SBSC55 membrane with 1.0 mm thickness under an air/He with oxygen partial pressure gradient over the temperature range of 600–800 °C is shown in Fig. 4(a). The oxygen permeation flux increased from $0.143 \text{ mL min}^{-1} \text{ cm}^{-2}$ at 500 °C to $0.406 \text{ mL min}^{-1} \text{ cm}^{-2}$ at 800 °C under synthetic air at a flow rate of 50 mL min^{-1} , helium at a rate of 25 mL min^{-1} . The reason could be ascribed to the facts that the oxygen permeation flux raised steadily with temperature because of the increase in oxygen ionic bulk diffusion, the surface exchange rate and oxygen vacancy concentration [39,40].

The ionic conductivity also could be evaluated via using the Wagner relationship based on the oxygen permeation flux results [41].

$$J(\text{O}_2) = \frac{RT}{16F^2L} \left(\frac{\sigma_e \sigma_i}{\sigma_e + \sigma_i} \right) (\ln P'_{\text{O}_2} - \ln P''_{\text{O}_2}) \quad (4)$$

where R is the ideal gas constant, L is the membrane thickness, T is the absolute temperature, F is the Faraday constant, σ_e is the electronic conductivity, σ_i is the oxygen ionic conductivity. P'_{O_2} and P''_{O_2} denote the oxygen partial pressure on the air side and the oxygen partial pressure on the sweep side, respectively. In this case, the conductivity of SBSC55 is totally dominated by electrical conductivity. σ_e is significantly great than σ_i so that Eq (4) could be rewritten as follows.

$$J(\text{O}_2) = \frac{RT}{16F^2L} (\sigma_i) (\ln P'_{\text{O}_2} - \ln P''_{\text{O}_2}) \quad (5)$$

The ionic conductivity can be estimated based on the oxygen permeation flux using the following equation.

$$\sigma_i = J(\text{O}_2) \frac{16F^2L}{RT} \left(\ln \frac{P'_{\text{O}_2}}{P''_{\text{O}_2}} \right)^{-1} \quad (6)$$

The calculated ionic conductivity is depicted in Fig. 4(a). The trend of ionic conductivity as a function of temperature is proportional to oxygen permeation flux. To further understand the oxygen migration process, the Arrhenius plot for oxygen permeation flux versus the reciprocal temperature was drawn. It was worthy to notice that the Arrhenius behavior for the oxygen permeation flux could be divided into two temperature regions (500–650 °C and 700–800 °C) as shown in Fig. 4(b). It was presumed that there are two different rate-determined processes (bulk diffusion process and slow surface exchange process) within two temperature

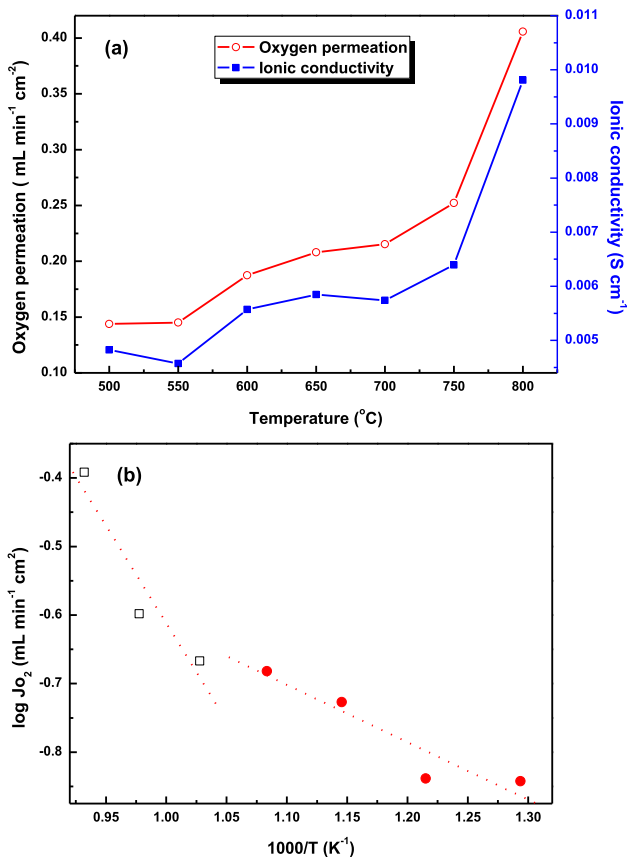


Fig. 4 – (a) Oxygen permeation flux and nominal ionic conductivities as a function of temperature for SBSC55 and (b) in the corresponding Arrhenius plot.

regions. Generally, for the entire oxygen diffusion activation energy, the slow surface exchange process with a higher activation energy compared with the bulk diffusion process. Based on the calculation of the slope of the Arrhenius plot, the activation energies for the high temperature region and low temperature region are 23.67 and 6.96 kJ mol^{-1} , respectively. It suggested that oxygen diffusion for high temperature range is surface exchange process, low temperature range is bulk diffusion process.

Thermogravimetric behavior and oxygen content ($5+\delta$)

To prove the oxygen content ($5+\delta$) for SBSC55, thermogravimetric analysis was carried out at various $p(\text{O}_2)$ in the range of 0.21 and 3.2×10^{-3} atm as a function of temperature as shown in Fig. 5. The weight loss upon heating was due to a partial loss of lattice oxygen and along with a reduction of Co^{4+} to Co^{3+} or Co^{3+} to Co^{2+} with increased temperature, so that the oxygen content, $5+\delta$, decreased with temperature [42–44]. It is seen that the magnitude of oxygen loss during heating was dependent on $p(\text{O}_2)$. With increasing the temperature, the weight loss and the magnitude of oxygen loss were gradually increased. Fig. 5(a) shows that slight weight loss from room temperature to 300 °C is attributed to desorption of the absorbed water from sample. When temperature increases above 300 °C, the

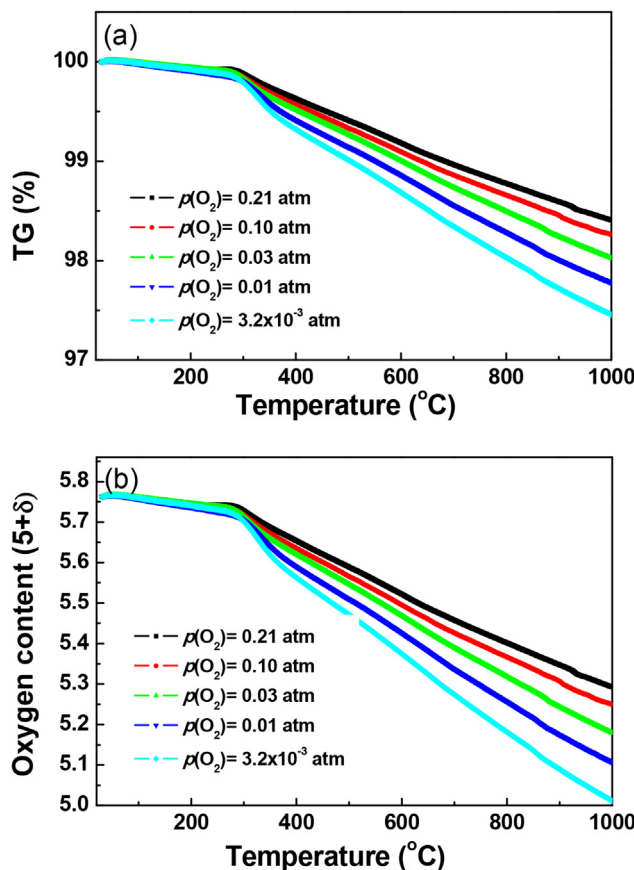


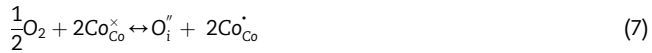
Fig. 5 – (a) Thermogravimetric data and (b) Oxygen content (5+ δ) data for SBSC55 cathode as a function of temperature with various oxygen atmosphere.

magnitude of weight loss is dramatic, implying that the specimen start to lose lattice oxygen significantly. A significant linear weight loss from 300 to 1000 °C indicates the lattice oxygen is gradually removed and the formation of additional oxygen vacancies [45]. With reducing $p(O_2)$ from 0.21 to 3.2×10^{-3} atm, the magnitude of weight loss is gradually significant especially as temperature above 300 °C, suggesting the escape of oxygen atoms from lattice and leading to decrease of oxygen content at lower $p(O_2)$. Based on iodometric titration result, the initial oxygen content (5+ δ) is 5.76 at room temperature. Fig. 5(b) shows the trend of oxygen content is as same as the weight loss as a function of temperature. At $p(O_2) = 0.21$ atm, the oxygen content of SBSC55 decreases gradually from 5.76 of 25 °C to 5.29 of 1000 °C. Similarly, at $p(O_2) = 3.2 \times 10^{-3}$ atm, the oxygen content significantly decreases from 5.76 of 25 °C to 5.01 of 1000 °C. The oxygen content decreased with decreasing $p(O_2)$, indicating that the amount of escape of oxygen atoms increases with decreasing $p(O_2)$. Table 2 listed the detailed oxygen content (5+ δ) as function of temperature with various $p(O_2)$.

Electrical conductivities and impedance spectra as function of oxygen partial pressures

Fig. 6 shows the temperature dependence of the electrical conductivity of the dense SBSC55 sample at $p(O_2) = 0.21$ and

0.01 atm. At $p(O_2) = 0.21$ atm, the conductivity significantly decreases with increasing temperature exhibiting a metallic behavior. It can be seen that an abrupt reduction of electrical conductivity from 300 °C due to lattice defects breaking the Co–O–Co bonds, resulting in escape of oxygen atoms from lattice and reduction of Co^{4+} to Co^{3+} or Co^{3+} to Co^{2+} , which corresponds to our previous TGA data. The apparent metallic conductivity behavior of SBSC55 may be related to the following reasons [46–48]: (1) an energy band overlap between Co-3d and O-2p; (2) the presence of Co^{4+} ions from thermally generated charge disproportion of Co^{3+} ; and (3) the loss of oxygen from the lattice at higher temperatures. At $p(O_2) = 0.01$ atm, the electrical conductivities decrease with decreasing $p(O_2)$, which is in agreement with the results of previous studies [49,50]. This is due to decreasing concentration of mobile interstitial oxygen at lower $p(O_2)$ [50]. In $SmBa_{0.5}Sr_{0.5}Co_2O_{5+\delta}$, the major defects are the oxygen interstitials, O_i'' and the electronic holes, $h = Co_{Co}^{\cdot}$ [51]. Using the Kroger–Vink notation, the formation of the oxygen interstitials and electronic hole is expressed by



The electrical neutrality condition is given by

$$2[O_i''] = [Co_{Co}^{\cdot}] \quad (8)$$

We can obtain the information from the neutrality condition that the decrease in the interstitial oxygen concentration by lowering $p(O_2)$ leads a reduction in electronic holes. The decrease in electronic holes is significantly related to lower electronic conductivities at lower $p(O_2)$. It is noted that the decreasing magnitude in electrical conductivity as a function of temperature for $p(O_2) = 0.01$ atm is much lower than $p(O_2) = 0.21$ atm. This indicates that the concentration of mobile interstitial oxygen is sensitive to temperature in air.

To further understand the effect of oxygen partial pressure, $p(O_2)$, on the cathode and mechanisms of oxygen reduction, EIS was investigated at different oxygen partial pressures. In general, the interfacial polarization resistance (R_p) changes with P_{O_2} can be described by the following equation [52,53]:

$$R_p = R_p^0 (P_{O_2})^{-n} \quad (9)$$

The overall ORR is expressed as follow.



Table 2 – The oxygen content (5+ δ) as a function of temperature with various oxygen atmospheres.

Oxygen partial pressure (atm)	Oxygen content (5+ δ)				
	Temperature (°C)				
	200 °C	400 °C	600 °C	800 °C	1000 °C
0.21	5.75	5.65	5.52	5.40	5.29
0.10	5.74	5.63	5.49	5.36	5.25
0.03	5.74	5.62	5.47	5.32	5.18
0.01	5.74	5.59	5.43	5.26	5.11
3.2×10^{-3}	5.74	5.56	5.37	5.18	5.01

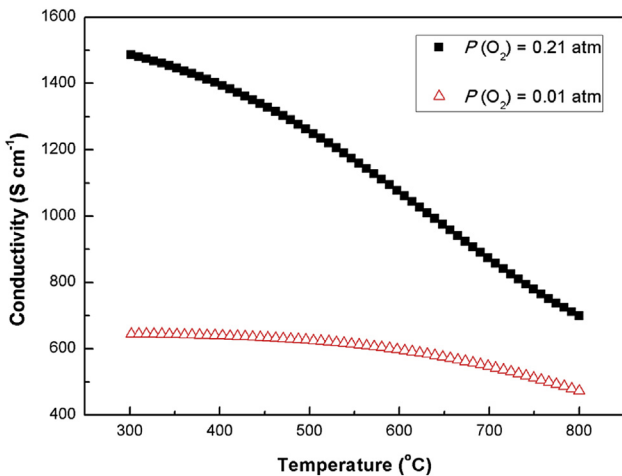
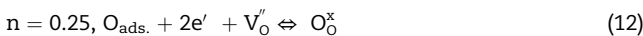
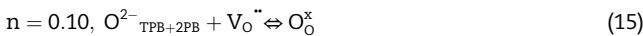


Fig. 6 – Temperature dependence of the electrical conductivity with various oxygen pressure.

The processes are complex containing charge transfer, surface adsorption/dissociation, gas diffusion, and so on. The magnitude of n provides valuable information about the rate-limiting step in the oxygen reduction reactions at cathodes [54,55]:



where $n = 0.10$ has been associated with oxygen ion transfer from triple-phase boundary (TPB) to the electrolyte, $n = 0.25$ with the charge transfer processes, $n = 0.50$ with oxygen adsorption/desorption processes, and $n = 1.00$ with gas phase diffusion of oxygen molecules in a porous cathode. However, the entire surface may serve as the active sites for ORR in MIEC conductors. It is ascribed to that oxygen ion can transport through the MIEC bulk [56,57]. Above-mentioned eq. (11) is mainly applied to pure electronic conductor, so that oxygen ion transfer is not only from TPB sites but also two-phase boundary (2PB) sites (cathode/electrolyte interface). In this case, Eq. (11) should be revised to following equation.



The R_p as a function of P_{O_2} for SBSC55 measured at various temperatures are shown in Fig. 7. Obviously, the R_p values increased with decreasing $P(O_2)$. This behavior is consistent with electrical conductivity at various $p(O_2)$ due to the decrease in mobile interstitial oxygen at lower $p(O_2)$. Based on slopes of $\log(R_p)$ vs. $\log(P_{O_2})$, the n values ranged from 0.10 to 0.17 in the

temperature range of 600–800 °C. This indicated that the rate-limiting mechanism of ORR is mostly dominated by oxygen ion transfer from TPB and/or two-phase boundary (2PB) sites at cathode with a small quantity of charge transfer reaction.

Long-term testing and polarization resistance

In order to evaluate the stability of the SBSC55|SDC|SBSC55 half-cell for a long time, the performance of a SBSC55|SDC|SBSC55 half-cell was tested, and the EIS and R_p were recorded as a function of time under stationary air as the oxidant at 600 °C as shown in Fig. 8. Obviously, R_p increased gradually with time, which values were increased from 4.17 Ω cm² for the initial 2 h to 5.37 Ω cm² for 96 h long-term testing at 600 °C. A slight increase in cathodic polarization resistance is observed with an increasing-rate around 0.30% h⁻¹ from the initial 2 h–96 h. Fig. 9(a) presents some typical impedance spectra of SBSC55 cathode measured in symmetrical cells using AC impedance spectrometry under open circuit condition ranged from 600 °C to 800 °C in air. The polarization resistances (R_p) of SBSC55 cathode reduced from 4.17 Ω cm² of 600 °C to 0.35 Ω cm² of 800 °C. Cathode delamination from electrolyte may be one possible cause of increasing in polarization resistance at initial fast degradation. Based on our group previous research, the difference in thermal expansion coefficient between SBSC55 and SDC is approximately 7.4 ppm K⁻¹ [58,59]. The delamination between layers causes the decline of reaction sites for ORR, leading to increase polarization resistance. With increasing the testing time, the following slow degradation in the MIEC-cathode performance may be several possible mechanisms such as (1) the grain size of SBSC55 may coarsen [60], (2) interdiffusion may occur between SBSC55 and SDC interface [61], and (3) Sr may segregate from Sr-contained cathode [62].

Exchange current density (i_o)

The exchange current density (i_o) value is an important information to evaluate the intrinsic oxygen reduction rate and

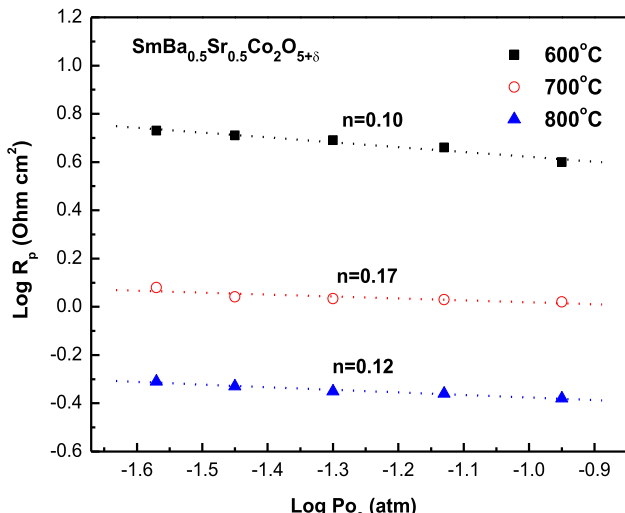


Fig. 7 – The interfacial polarization resistance (R_p) as a function of oxygen partial pressure for SBSC55 cathode measured in the temperature range of 600–800 °C.

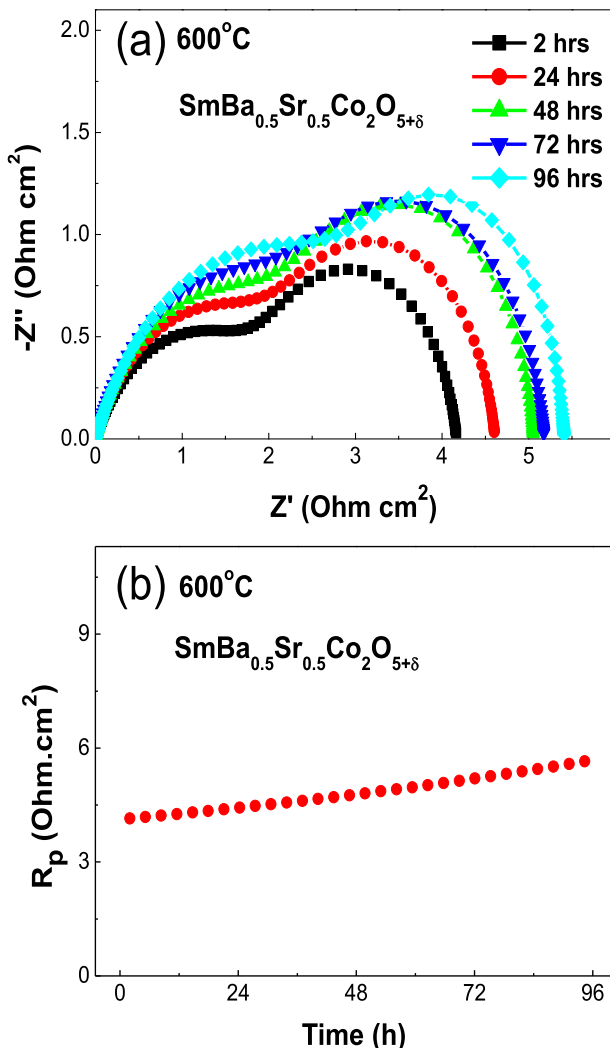


Fig. 8 – Long-term testing for a SBSC55|SDC|SBSC55 half-cell at 600 °C: (a) Nyquist diagram of the impedance spectroscopy and (b) polarization resistance (R_p).

the electrochemical properties of cathode. The i_o value is proportional to the capacity of oxygen reduction reaction for cathode. The i_o values could be acquired via different testing techniques. In the present work, the i_o values were identified using electrochemical impedance spectrometry (EIS), low-field (LF) and high-field (HF) techniques. For EIS technique, i_o values were determined from the R_p of the Nyquist plot as depicted in Fig. 9(a). For LF technique, i_o values were identified from the slope of the i vs. η plots as shown in Fig. 9(b). For HF technique, i_o values can be obtained from the y-intercept of i vs. η plots as shown in Fig. 9(c). The detailed information regarding these techniques could refer to our group published paper [27].

The i_o values of SBSC55 identified via EIS, LF and HF technique are summarized in Table 3. Generally, the i_o values are rising with temperature. The i_o values were increased from 4.5 mA cm^{-2} of 600 °C to 64.2 mA cm^{-2} of 800 °C for EIS technique, the i_o values were rising from 2.6 mA cm^{-2} of 600 °C to 16.5 mA cm^{-2} of 800 °C for LF and the i_o values were enhanced from 7.6 mA cm^{-2} of 600 °C to 50.8 mA cm^{-2} of

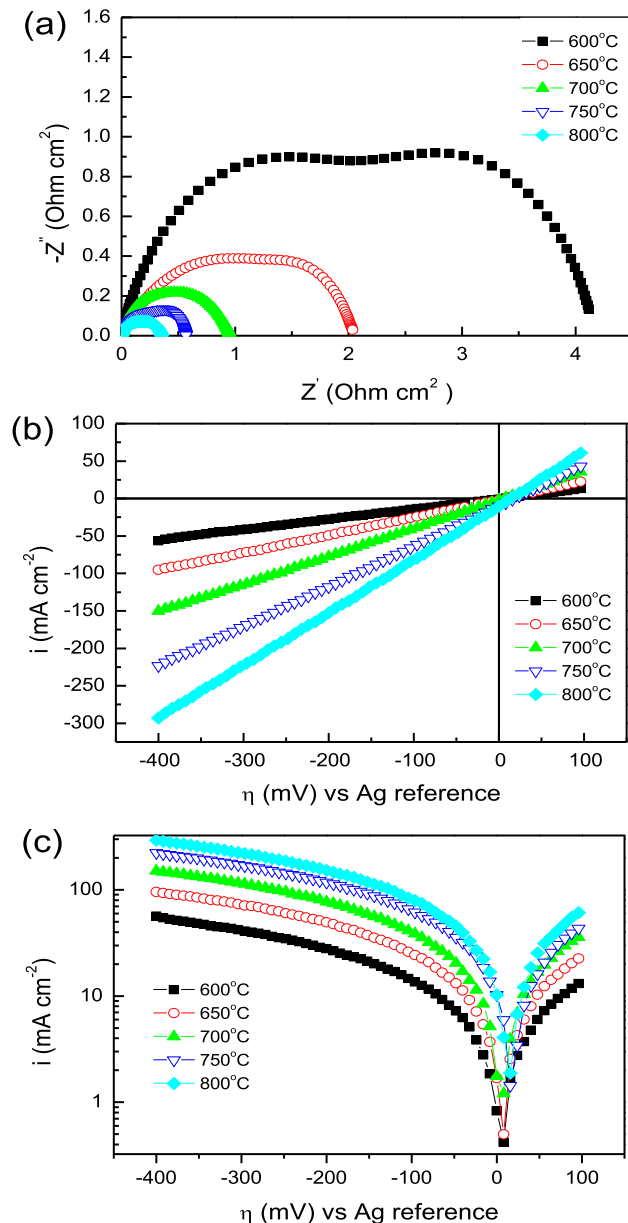


Fig. 9 – (a) Nyquist plots of EIS, (b) Cyclic voltammogram and (c) Tafel plots at 0.5 mVs^{-1} between 100 mV and -400 mV of SBSC55 cathode on SDC electrolyte over the temperature range of $600\text{--}800 \text{ }^\circ\text{C}$.

800 °C for HF. The overall activation energy (E_a) for the ORR was identified from the slope of the Arrhenius plots, as shown in the following equation.

$$\ln i_o = \ln K - \frac{E_a}{RT} \quad (16)$$

where K is the pre-exponential constant, which can be calculated from the y-intercept, and E_a is the reaction activation energy. Fig. 10 exhibited the Arrhenius plots for i_o values for SBSC55 ranged from 600 °C to 800 °C. The E_a values identified via EIS, LF and HF techniques were 172.9, 68.9 and 70.2 kJ mol^{-1} , respectively. The linearity of the Arrhenius plots implying that SBSC55 cathode is stable as a function of temperature. The

Table 3 – Exchange current density, i_o of ORR for the $\text{SmBa}_{0.5}\text{Sr}_{0.5}\text{Co}_2\text{O}_{5+\delta}$ cathode using EIS, low-field and high-field techniques over the temperature range of 600–800 °C.

T(°C)	i_o (mA cm ⁻²)		
	EIS	LF	HF
600	4.5	2.6	7.6
650	9.7	4.8	14.1
700	22.1	8.0	23.1
750	38.7	12.3	39.5
800	64.2	16.5	50.8

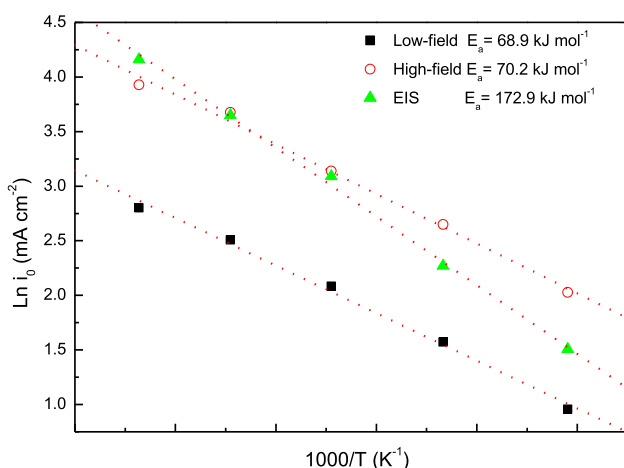


Fig. 10 – Arrhenius plots of ORR for SBSC55 cathode, i_o was obtained using the EIS, low-field and high-field technique.

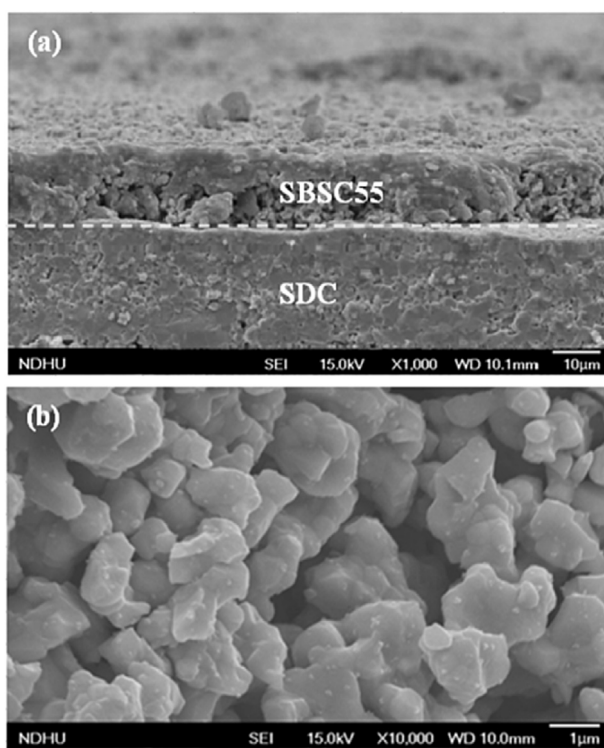


Fig. 11 – SEM image SBSC55|SDC half cell: (a) cross-section view and (b) surface view of SBSC55 cathode.

activation value is relatively similar to our previous report as cited in Ref. [27], it indicates that SBSC55 is a candidate cathode for SOFCs due to its highly electrocatalytic activity.

SEM images

The cathode microstructure is closely related to the electron and oxygen transportation. These properties influence the performance of fuel cell such as the reaction kinetics, charge transport, and mass transport preprocess [63,64]. The microstructure of a cross-section of SBSC55|SDC half cell and surface view of SBSC55 cathode as shown in Fig. 11 revealed SBSC55 cathode with a thickness of 15 μm, and the adhesion between the cathode and electrolyte is quite good. The SBSC55 particles distributed uniformly, and the particle size ranged from 1 to 2 μm.

Conclusions

This study mainly investigated structural characteristics, thermogravimetric behavior, oxygen non-stoichiometry, oxygen permeation, electrical conductivity, chemical bulk diffusion coefficient (D_{chem}), electrochemical properties and long-term testing for SBSC55 cathode. The weight loss upon heating was due to a partial loss of lattice oxygen and along with a reduction of Co^{4+} to Co^{3+} or Co^{3+} to Co^{2+} with increased temperature, so that the oxygen content ($5+\delta$) decreased with temperature. The conductivity significantly decreases with increasing temperature exhibiting a metallic behavior. The oxygen permeation flux for SBSC55 membrane with 1.0 mm thickness was in the range of 0.143–0.406 mL min⁻¹ cm⁻², and the ionic conductivity was in the range of 0.0048–0.0098 S cm⁻¹ from 500 °C to 800 °C under air at a flow rate of 50 mL min⁻¹, helium at a rate of 25 mL min⁻¹. The D_{chem} values for SBSC55 cathode are in the range of 2.6×10^{-6} – 1.8×10^{-5} cm² s⁻¹ from 500 °C to 700 °C with activation energy of 57.96 kJ mol⁻¹. For long-term testing, R_p of SBSC55 was gradually increased from $4.17 \Omega \text{ cm}^2$ to $5.37 \Omega \text{ cm}^2$ after 96 h testing at 600 °C with an increase rate of 0.30% h⁻¹. Therefore, $\text{SmBa}_{0.5}\text{Sr}_{0.5}\text{Co}_2\text{O}_{5+\delta}$ is desirable candidate cathode materials in IT-SOFCs in accordance with electrochemical performance. The rate-limiting step of ORR is the majority of the oxygen ion transfer from TPB and/or 2PB sites of cathode with the minority of charger transfer reaction.

Acknowledgements

The authors are grateful for the financial support of this research by Ministry of Science and Technology of Taiwan under contract number: MOST 104-2119-M-259-003 and MOST 104-2113-M-259-005.

REFERENCES

- [1] Ding D, Li X, Lai SY, Gerdes K, Liu M. Enhancing SOFC performance by surface modification through infiltration. Energy Environ Sci 2014;7:552–75.

- [2] Moon H, Kim SD, Hyun SH, Kim HS. Development of IT-SOFC unit cells anode-supported thin electrolytes via tape casting and co-firing. *Int J Hydrogen Energy* 2008;33:1758–68.
- [3] Colomer MT, Steele BCH, Kilner JA. Structural and electrochemical properties of the $\text{Sr}_{0.8}\text{Ce}_{0.1}\text{Fe}_{0.7}\text{Co}_{0.3}\text{O}_{3-\delta}$ perovskite as cathode material for IT-SOFCs. *Solid State Ionics* 2002;147:41–8.
- [4] Brandon NP, Skinner SJ, Steele BCH. Recent advances in materials for fuel cells. *Ann Rev Mater Res* 2003;33:182–213.
- [5] Zhou Q, He T, Ji Y. $\text{SmBaCo}_2\text{O}_{5+\delta}$ double-perovskite structure cathode material for intermediate-temperature solid-oxide fuel cells. *J Power Sources* 2008;185:754–8.
- [6] Chen DJ, Ran R, Zhang K, Wang J, Shao ZP. Intermediate-temperature electrochemical performance of a polycrystalline $\text{PrBaCo}_2\text{O}_{5+\delta}$ cathode on samarium-doped ceria electrolyte. *J Power Sources* 2009;188:96–105.
- [7] Zhao F, Wang S, Brinkman K, Chen F. Layered perovskite $\text{PrBa}_{0.5}\text{Sr}_{0.5}\text{Co}_2\text{O}_{5+\delta}$ as high performance cathode for solid oxide fuel cells using oxide proton-conducting electrolyte. *J Power Sources* 2010;195:5468–73.
- [8] Sindirac C, Akkurt S. Formation of $\text{La}_{1-x}\text{Sr}_x\text{Co}_{1-y}\text{Fe}_y\text{O}_3-\delta$ cathode materials from precursor salts by heating in contact with CGO electrolyte. *Int J Hydrogen Energy* 2016;41:18157–65.
- [9] Tarancón A, Burriel M, Santiso J, Skinner SJ, Kilner JA. Advances in layered oxide cathodes for intermediate temperature solid oxide fuel cells. *J Mater Chem* 2010;20:3799–813.
- [10] Lee Y, Kim DY, Choi GM. $\text{GdBaCo}_2\text{O}_{5+x}$ cathode for anode-supported ceria SOFCs. *Solid State Ionics* 2011;192:527–30.
- [11] Liu Y, Bi J, Chi B, Pu J, Jian L. Effects of impregnating palladium on catalytic performance of LSCF-GDC composite cathodes for intermediate temperature solid oxide fuel cells. *Int J Hydrogen Energy* 2016;41:6484–92.
- [12] Frontera C, Caneiro A, Carrillo AE, Oró-Solé J, García-Muñoz JL. Tailoring oxygen content on $\text{PrBaCo}_2\text{O}_{5+\delta}$ layered cobaltites. *Chem Mater* 2005;17:5439–45.
- [13] Parfitt D, Chroneos A, Tarancón A, Kilner JA. Oxygen ion diffusion in cation ordered/disordered $\text{GdBaCo}_2\text{O}_{5+\delta}$. *J Mater Chem* 2011;21:2183–6.
- [14] Pang S, Wang W, Chen T, Wang Y, Xu K, Shen X, et al. The effect of potassium on the properties of $\text{PrBa}_{1-x}\text{Co}_2\text{O}_{5+\delta}$ ($x=0.00-0.10$) cathodes for intermediate-temperature solid oxide fuel cells. *Int J Hydrogen Energy* 2016;41:13705–14.
- [15] Kim JH, Irvine JTS. Characterization of layered perovskite oxides $\text{NdBa}_{1-x}\text{Sr}_x\text{Co}_2\text{O}_{5-\delta}$ ($x=0$ and 0.5) as cathode materials for IT-SOFC. *Int J Hydrogen Energy* 2012;37:5920–9.
- [16] Kuroda C, Zheng K, Swierczek K. Characterization of novel $\text{GdBa}_{0.5}\text{Sr}_{0.5}\text{Co}_{2-x}\text{Fe}_x\text{O}_{5+\delta}$ perovskites for application in IT-SOFC cells. *Int J Hydrogen Energy* 2013;38:1027–38.
- [17] Kim J, Jun A, Shin J, Kim G. Effect of Fe doping on layered $\text{GdBa}_{0.5}\text{Sr}_{0.5}\text{Co}_2\text{O}_{5+\delta}$ perovskite cathodes for intermediate temperature solid oxide fuel cells. *J Am Ceram Soc* 2014;97:651–6.
- [18] Jiang L, Wei T, Zeng R, Zhang WX, Huang YH. Thermal and electrochemical properties of $\text{PrBa}_{0.5}\text{Sr}_{0.5}\text{Co}_{2-x}\text{Fe}_x\text{O}_{5+\delta}$ ($x=0.5, 1.0, 1.5$) cathode materials for solid-oxide fuel cells. *J Power Sources* 2013;232:279–85.
- [19] Xue J, Shen Y, He T. Performance of double-perovskite $\text{YBa}_{0.5}\text{Sr}_{0.5}\text{Co}_2\text{O}_{5-\delta}$ as cathode material for intermediate-temperature solid oxide fuel cells. *Int J Hydrogen Energy* 2011;36:6894–8.
- [20] Kim JH, Cassidy M, Irvine JTS, Bae J. Advanced electrochemical properties of $\text{LnBa}_{0.5}\text{Sr}_{0.5}\text{Co}_2\text{O}_{5+\delta}$ ($\text{Ln}=\text{Pr}, \text{Sm}, \text{and Gd}$) as cathode materials for IT-SOFC. *J Electrochem Soc* 2009;156:B682–9.
- [21] Kim JH, Cassidy M, Irvine JTS, Bae J. Electrochemical investigation of composite cathodes with $\text{SmBa}_{0.5}\text{Sr}_{0.5}\text{Co}_2\text{O}_{5+\delta}$ cathodes for intermediate temperature-operating solid oxide fuel cell. *Chem Mater* 2010;22:883–92.
- [22] Jun A, Kim J, Shin J, Kim G. Optimization of Sr content in layered $\text{SmBa}_{1-x}\text{Sr}_x\text{Co}_2\text{O}_{5+\delta}$ perovskite cathodes for intermediate-temperature solid oxide fuel cells. *Int J Hydrogen Eng* 2012;37:18381–8.
- [23] Wang B, Long G, Li Y, Ji Y. Characterization of $\text{SmBa}_{0.5}\text{Sr}_{0.5}\text{CoCu}_2\text{O}_{5+\delta}$ cathode based on GDC and LSMG electrolyte for intermediate-temperature solid oxide fuel cells. *Int J Hydrogen Energy* 2016;41:13603–10.
- [24] McKinlay A, Connor P, Irvine JTS, Zhou WZ. Structural chemistry and conductivity of solid solution $\text{YBa}_{1-x}\text{Sr}_x\text{Co}_2\text{O}_{5+\delta}$. *J Phys Chem C* 2007;111:19120–5.
- [25] Kim JH, Prado F, Manthiram A. Characterization of $\text{GdBa}_{1-x}\text{Sr}_x\text{Co}_2\text{O}_{5+\delta}$ ($0 \leq x \leq 1.0$) double perovskites as cathodes for solid oxide fuel cells. *J Electrochem Soc* 2008;155:B1023–8.
- [26] Kim JH, Manthiram A. Layered $\text{LnBaCo}_2\text{O}_{5+\delta}$ perovskite cathodes for solid oxide fuel cells: an overview and perspective. *J Mater Chem A* 2015;3:24195–210.
- [27] Subardi A, Cheng MH, Fu YP. Chemical bulk diffusion and electrochemical properties of $\text{SmBa}_{0.6}\text{Sr}_{0.4}\text{Co}_2\text{O}_{5+\delta}$ cathode for intermediate solid oxide fuel cells. *Int J Hydrogen Energy* 2014;39:20783–90.
- [28] Fu YP, Wen SB, Lu CH. Preparation and characterization of samaria-doped ceria electrolyte materials for solid oxide fuel cells. *J Am Ceram Soc* 2008;91:127–31.
- [29] Kuhn M, Kim JJ, Bishop SR, Tuller HL. Oxygen nonstoichiometry and defect chemistry of perovskite-structured $\text{Ba}_{x}\text{Sr}_{1-x}\text{Ti}_{1-y}\text{Fe}_y\text{O}_{3-y/2+\delta}$ solid solutions. *Chem Mater* 2013;25:2970–5.
- [30] Nadalin RJ, Brozda WB. Chemical methods for the determination of the “oxidizing (or reducing) power” of certain materials containing a multivalent element in several oxidation states. *Anal Chim Acta* 1963;28:282–93.
- [31] Fu YP, Ouyang J, Li CH, Hu SH. Chemical bulk diffusion coefficient of $\text{Sm}_{0.5}\text{Sr}_{0.5}\text{CoO}_{3-\delta}$ cathode for solid oxide fuel cells. *J Power Sources* 2013;240:168–77.
- [32] Chen Y, Qian B, Li S, Jiao Y, Tade MO, Shao Z. The influence of impurity ions on the permeation and oxygen reduction properties of $\text{Ba}_{0.5}\text{Sr}_{0.5}\text{Co}_{0.8}\text{Fe}_{0.2}\text{O}_{3-\delta}$ perovskite. *J Membr Sci* 2014;449:86–96.
- [33] Jun A, Shin J, Kim G. High redox and performance stability of layered $\text{SmBa}_{0.5}\text{Sr}_{0.5}\text{Co}_{1.5}\text{Cu}_{0.5}\text{O}_{5+\delta}$ perovskite cathodes for intermediate-temperature solid oxide fuel cells. *Phys Chem Chem Phys* 2013;15:19906–12.
- [34] Elshof JE, Lankhorst MHR, Bouwmeester HJM. Oxygen exchange and diffusion coefficients of strontium-doped lanthanum ferrites by electrical conductivity relaxation. *J Electrochem Soc* 1997;144:1060–7.
- [35] Huang C, Chen D, Lin Y, Ran R, Shao Z. Evaluation of $\text{Ba}_{0.6}\text{Sr}_{0.4}\text{Co}_{0.9}\text{Nb}_{0.1}\text{O}_{3-\delta}$ mixed conductor as a cathode for intermediate-temperature oxygen-ionic solid-oxide fuel cells. *J Power Sources* 2010;195:5176–84.
- [36] Chen D, Shao Z. Surface exchange and bulk diffusion properties of $\text{Ba}_{0.6}\text{Sr}_{0.4}\text{Co}_{0.9}\text{Nb}_{0.1}\text{O}_{3-\delta}$ mixed conductor. *Int J Hydrogen Energy* 2011;36:6948–56.
- [37] Choi MB, Lee KT, Yoon HS, Jeon SY, Wachsman ED, Song SJ. Electrochemical properties of ceria-based intermediate temperature solid oxide fuel cell using microwave heat-treated $\text{La}_{0.1}\text{Sr}_{0.9}\text{Co}_{0.8}\text{Fe}_{0.2}\text{O}_{3-\delta}$ as a cathode. *J Power Sources* 2012;220:377–82.
- [38] Kim G, Wang S, Jacobson AJ, Reimus L, Brodersen P, Mims CA. Rapid oxygen ion diffusion and surface exchange kinetics in $\text{PrBaCo}_2\text{O}_{5+x}$ with a perovskite related structure and ordered A cations. *J Mater Chem* 2007;17:2500–5.
- [39] Han D, Wu J, Yan Z, Zhang K, Liu J, Liu S. $\text{La}_{0.6}\text{Sr}_{0.4}\text{Co}_{0.2}\text{Fe}_{0.8}\text{O}_{3-\delta}$ hollow fibre membrane performance

- improvement by coating of $\text{Ba}_{0.5}\text{Sr}_{0.5}\text{Co}_{0.9}\text{Nb}_{0.1}\text{O}_{3-\delta}$ porous layer. *RSC Adv* 2014;4:19999–20004.
- [40] Yang J, Zhao H, Liu X, Shen Y, Xu L. Bismuth doping effects on the structure, electrical conductivity and oxygen permeability of $\text{Ba}_{0.6}\text{Sr}_{0.4}\text{Co}_{0.7}\text{Fe}_{0.3}\text{O}_{3-\delta}$ ceramic membranes. *Int J Hydrogen Energy* 2012;37:12694–9.
- [41] Wiik K, Aasland S, Hansen HL, Tangen IL, Ødegard R. Oxygen permeation in the system $\text{SrFeO}_{3-x}\text{-SrCoO}_{3-y}$. *Solid State Ionics* 2002;152–153:675–80.
- [42] Meuffels P. Propane gas sensing with high-density $\text{SrTi}_{0.6}\text{Fe}_{0.4}\text{O}_{(3-\delta)}$ ceramics evaluated by thermogravimetric analysis. *J Eur Ceram Soc* 2007;27:285–90.
- [43] Lia S, Jin W, Xu N, Shi J. Mechanical strength, and oxygen and electronic transport properties of $\text{SrCo}_{0.4}\text{Fe}_{0.6}\text{O}_{3-\delta}$ -YSZ membranes. *J Membr Sci* 2001;186:195–204.
- [44] Wei B, Lü Z, Li S, Liu Y, Liu K, Su W. Thermal and electrical properties of new cathode material $\text{Ba}_{0.5}\text{Sr}_{0.5}\text{Co}_{0.8}\text{Fe}_{0.2}\text{O}_{3-\delta}$ for solid oxide fuel cells. *Electrochim Solid State Lett* 2005;8:A428–31.
- [45] Kostogloudis GCh, Vasilakos N, Ftikos Ch. Crystal structure, thermal and electrical properties of $\text{Pr}_{1-x}\text{Sr}_x\text{CoO}_{3-\delta}$ ($x=0, 0.15, 0.3, 0.4, 0.5$) perovskite oxides. *Solid State Ionics* 1998;106:207–18.
- [46] Park S, Choi S, Shin J, Kim G. Tradeoff optimization of electrochemical performance and thermal expansion for Co-based cathode material for intermediate-temperature solid oxide fuel cells. *Electrochim Acta* 2014;125:683–90.
- [47] Zhang X, Hao H, Hu X. Electronic transport properties of $\text{YBaCo}_{2-x}\text{Cu}_x\text{O}_{5+\delta}$ ($0 \leq x \leq 1$) at high temperature. *Phys Rev B* 2008;403:3406–9.
- [48] Yoo S, Shin JY, Kim G. Thermodynamic and electrical characteristics of $\text{NdBaCo}_2\text{O}_{5+\delta}$ at various oxidation and reduction states. *J Mat Chem* 2011;21:439–43.
- [49] Choi S, Shin J, Kim G. The electrochemical and thermodynamic characterization of $\text{PrBaCo}_{2-x}\text{Fe}_x\text{O}_{5+\delta}$ ($x = 0, 0.5, 1$) infiltrated into yttria-stabilized zirconia scaffold as cathodes for solid oxide fuel cells. *J Power Sources* 2012;201:10–7.
- [50] Mauvy F, Bassat JM, Boehm E, Manaud JP, Dordor P, Grenier JC. Oxygen electrode reaction on $\text{Nd}_2\text{NiO}_{4+\delta}$ cathode materials: impedance spectroscopy study. *Solid State Ionics* 2003;158:17–28.
- [51] Vashook VV, Tolochko SP, Yushkevich II, Makhnach LV, Kononyuk IF, Altenburg H, et al. Oxygen nonstoichiometry and electrical conductivity of the solid solutions $\text{La}_{2-x}\text{Sr}_x\text{NiO}_y$ ($0 \leq x \leq 0.5$). *Solid State Ionics* 1998;110:245–53.
- [52] Takeda Y, Kanno R, Noda M, Tomida Y, Yamamoto O. Cathodic polarization phenomena of perovskite oxide electrodes with stabilized zirconia. *J Electrochem Soc* 1987;134:2656–61.
- [53] Jaiswal A, Wachsman ED. Bismuth-ruthenate-based cathodes for IT-SOFCs. *J Electrochem Soc* 2005;152:A787–90.
- [54] Fukunaga H, Koyama M, Takahashi N, Wen C, Yamada K. Reaction model of dense $\text{Sm}_{0.5}\text{Sr}_{0.5}\text{CoO}_3$ as SOFC cathode. *Solid State Ionics* 2000;132:279–85.
- [55] Meng FC, Xia T, Wang J, Shi Z, Lian JP, Zhao H, et al. Evaluation of layered perovskites $\text{YBa}_{1-x}\text{Sr}_x\text{Co}_2\text{O}_{5+\delta}$ as cathodes for intermediate- temperature solid oxide fuel cells. *Int J Hydrogen Energy* 2014;39:4531–43.
- [56] Kim J, Seo WY, Shin J, Liu M, Kim G. Composite cathodes composed of $\text{NdBa}_{0.5}\text{Sr}_{0.5}\text{Co}_2\text{O}_{5+\delta}$ and $\text{Ce}_{0.9}\text{Gd}_{0.1}\text{O}_{1.95}$ for intermediate-temperature solid oxide fuel cells. *J Mater Chem A* 2013;1:515–9.
- [57] Irvine JTS, Neagu D, Verbraeken MC, Chatzichristodoulou C, Graves C, Mogensen MB. Evolution of the electrochemical interface in high-temperature fuel cells and electrolyzers. *Nat Energy* 2016, 15014.
- [58] Subardi A, Chen CC, Cheng MH, Chang WK, Fu YP. Electrical, thermal and electrochemical properties of $\text{SmBa}_{1-x}\text{Sr}_x\text{Co}_2\text{O}_{5+\delta}$ cathode materials for intermediate-temperature solid oxide fuel cells. *Electrochim Acta* 2016;204:118–27.
- [59] Fu YP, Chen RH, Hsieh MY, Subardi A, Chang WK. Double perovskite $\text{LaSrCo}_{1.6}\text{Cu}_{0.4}\text{O}_{5+\delta}$ cathode for IT-SOFCs with pulsed laser technique deposited bi-layer electrolyte. *J Electrochem Soc* 2015;162:F1029–35.
- [60] Call AV, Railsback JG, Wang H, Barnett SA. Degradation of nano-scale cathodes: a new paradigm for selecting low- temperature solid oxide cell materials. *Phys Chem Chem Phys* 2016;18:13216–22.
- [61] Chen K, Jiang SP. Review-materials degradation of solid oxide electrolysis cells. *J Electrochem Soc* 2016;163:F3070–83.
- [62] Jung WC, Tuller HL. Investigation of surface Sr segregation in model thin film solid oxide fuel cell perovskite electrodes. *Energy Environ Sci* 2012;5:5370–8.
- [63] Nam JH, Jeon DH. A comprehensive microscale model for transport and reaction in intermediate temperature solid oxide fuel cell. *Electrochim Acta* 2006;51:3446–60.
- [64] Andersson M, Yuan J, Sundén B. Review on modeling development for multiscale chemical reactions coupled transport phenomena in solid oxide fuel cell. *Appl Energy* 2010;87:1461–76.